Overview of Laser Ablation Micropropulsion Research Activities at DLR Stuttgart

Hans-Albert Eckel, Stefan Scharring, Stephanie Karg, Christian Illg, and Johannes Peter

Institute of Technical Physics, German Aerospace Center (DLR), Pfaffenwaldring 38 – 40, 70569 Stuttgart, Germany

Abstract. Microthrust engines (μN-mN) with high specific impulse and long lifetime that allow for precision attitude and orbit control are a prerequisite for planned and future missions for geodetic purposes or astronomic science. The potential of laser-ablative microthrusters for meeting these demands is being investigated at the Institute of Technical Physics. The concept is based on removal of a thin layer of material by focusing short laser pulses on a metal surface creating plasma or vapor. The recoil of the ablated material leads to momentum transfer to the target, which results in sub-μN to mN thrust levels for high repetition rate laser sources. Additionally, by implementing electro-optic beam steering for layer-by-layer ablation of material, moving parts that can be a significant disturbing factor for precise thrusters could be avoided in this concept. To evaluate and optimize the thruster with regards to precise thrust control, thruster lifetime and contamination issues experimental facilities comprising plasma and surface diagnostics and a thrust balance have been implemented. In addition to the experimental work, analytical calculations are undertaken to assess the future laser thruster characteristics. Furthermore, the variation of laser parameters and target material is investigated using a hydrodynamic simulation tool for laser ablation, which is to be supplemented by molecular dynamics simulations as well as by Direct Simulation Monte Carlo-Particle in Cell (DSMC-PIC) calculations in cooperation with the University of Stuttgart.

Keywords: Laser ablation of solids, Laser ablation microthruster, Plasma diagnostic techniques, Electro-optical components, Hydrodynamic simulations, Direct Simulation Monte Carlo, Particle-in-cell method
PACS: 42.15.Eq, 52.65.Pp, 52.65.Kj, 52.65.Rr, 52.70.-m, 79.20.Eb

1. INTRODUCTION

As a special case of electric micropropulsion, laser ablative thruster concepts have extensively been explored in the last years. Basically, the recoil of the ablation plume by a propellant target under pulsed laser ablation yields an impulse bit that can be tailored to mission demands by optimization of laser fluence, pulse length, wavelength and ablation material, whereas the resulting thrust might be varied over several orders of magnitude by adjusting the laser repetition rate, i.e. the number of impulse bits/second [1].

Concepts of technical realization can be divided into T-mode (transmission) and R-mode (reflection) thrusters, where in the first case the laser illuminates the propellant material through a transparent substrate for optics protection yielding an ablation jet

coaxial to the laser beam [2]. In the latter case, the laser is directed in oblique incidence to the target surface yielding an ablation jet perpendicular to it [3].

In these concepts, however, propellant supply is often realized by mechanical transport mechanisms, e.g. an ablation target tape [2] or a rotating hard disc device [3]. This may result in non-negligible residual momentum that is imparted to the spacecraft increasing the noise-equivalent thrust level of the propulsion device. However, especially in scientific missions, e.g. GRACE, MICROSCOPE or LISA, high-precision formation flight of satellite formations and / or accurate control of orbit and attitude may require an extremely low residual acceleration below 10^{-14} m $s^{-2}/\sqrt{\text{Hz}}$ [4].

Hence, in order to realize very low thrust levels precisely and free of noise, in the DLR concept of laser ablative micropropulsion, we intend to realize Arthur Kantrowitz' "4P-principle": Payload – Propellant – Photons – Period, in a puristic way:

1. **Photonic** motion is only affected by stimulated emission, reflection, and refraction.
2. The motion of the **propellant** is exclusively due to laser ablation.
3. The **payload**'s motion results solely from the recoil of the ablation jet.
4. **Period**. Nothing else moves.

Whereas these principles should provide for a very low thrust noise level, the following requirements can be deduced:

1. The optical setup must avoid moving elements, e.g. turnable mirrors.
2. In repetitive operation, propellant cannot be supplied to the laser-matter interaction area, but the laser focus has to follow the propellant surface being consumed during thruster operation.
3. In general, the thruster concept has to meet the requirement of "no moving parts", e.g. no valves.

Therefore, in our research, the development of an electro-optical beam steering as well as studies on surface quality of the target after ablation are highly significant. As in any field of laser propulsion, however, experimental analyses as well as simulations of laser-induced momentum and the propagation of the ablation plume remain relevant as well.

In the following, an overview of the status in these research topics at DLR Stuttgart is given.

2. LASER-ABLATIVE MICROLAS THRUSTER

A. Thruster concept

In Fig. 1 a sketch of the MICROLAS thruster is shown: The beam of a pulsed microchip laser is focused by an f-theta lens (O) to the metallic surface (T). Optics contamination is prevented by reflection of the beam at a plane mirror (M). Residual contamination by the divergent plume may occur here, however, the corresponding detrimental effects might by minimized by choosing the same material for target and mirror.

Variation of the laser spot position is enabled by electro-optical elements (EO2) which provide for 2D lateral shift of the beam. With a suitable hatching pattern, the target can be ablated layer by layer which is comparable to laser milling [5].

Whereas a fixed focus length is already given by the f-theta lens (O), slight variations of the overall focus length can be realized by an electro-optical lens taking into account for the changing position of the target surface under ablation of the target layer by layer.

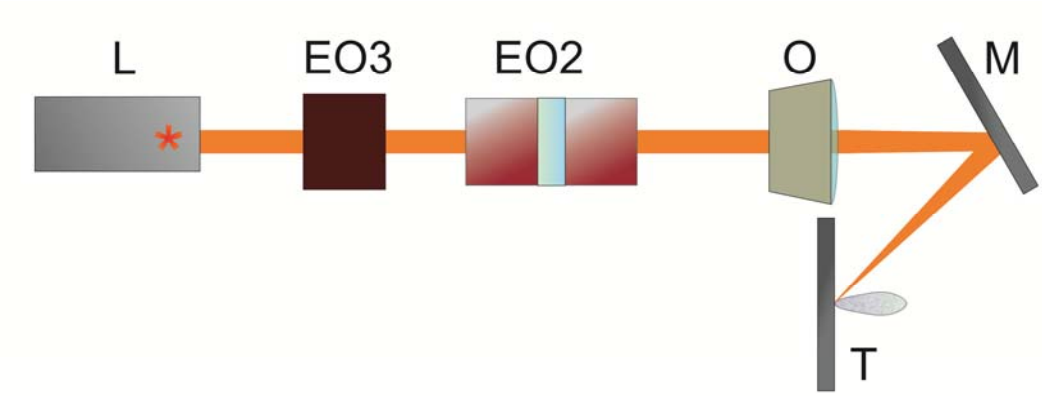

FIGURE 1. Concept of the MICROLAS laser ablative thruster comprising a pulsed microchip laser (L), an electro-optical lens (EO3) with variable focus length, an electro-optical device (EO2) for 2D lateral beam-steering, an f-theta lens with fixed focus length, a plane mirror (M), and a metallic target (T).

B. Research strategy

1. Laser sources and beam-steering

Microchip lasers, which provide sufficiently high pulse energies and short pulse lengths for ablation of metal targets in a relatively small package, are the most likely suitable candidates for use in an actual thruster application and are as a result the main type of laser used in the experimental work. Two microchip lasers with 1064 nm wavelength, a measured M^2 of approx. 1.8 and different pulse lengths and energies (1 ns at max. 1 mJ and 500 ps at max. 80 µJ) are currently being used in ablation experiments. Additionally a Nd:YVO_4 slab laser that provides a greater range of pulse energies (up to 7 mJ) and repetition rates (up to 40 kHz) at 8 – 10 ns pulse length and 1064 nm wavelength is used for thrust measurements. Control of the laser ablation pattern is currently realized in two ways: in plume diagnostics experiments by moving the target and for thrust measurements by using a 2D-galvanometer-scanner and f-theta lens setup. One promising technology for 3D-electro-optic beam steering are KTN crystal scanners and lenses developed by NTT-AT [6, 7, 8]. 1D-KTN modules are currently being tested and evaluated with regard to their potential for 2D-beam steering.

2 Laser-induced momentum coupling

Laser-induced momentum is measured using a torsional pendulum balance with a total arm length of 250 mm and flexural pivots as torsional element. Voice coils are used for calibration and as force actuator for closed-loop operation. A more detailed description of the thrust balance and the experimental facilities mentioned in the following sections is given in [9, 10].

1D hydrodynamic simulations on laser ablation of aluminum are carried out for a great set of optical parameters using the Virtual Laser Lab (VLL) [11], which employs the Two-Temperature Model for laser matter interaction and the Helmholtz equation to take into account for the temporal evolution of permittivity changes inside the material with a high spatial resolution, as described in detail in [12]. Post-processing of the results comprising e.g. velocity distribution of the ablation jet and information on phase transitions allows for the determination of typical figures of merit like impulse coupling coefficient and specific impulse.

Molecular Dynamics (MD) simulations with IMD from the University of Stuttgart were tested as well but have been found to be suitable for laser pulses in the femtosecond range only [13].

3. Plume diagnostics

Analysis of the plasma plume that results from each ablation event is useful for gaining a better understanding of the laser ablation process and assessing the influence of changing surface roughness and contamination issues. In the current experimental setup information on charged plume components can be obtained from Faraday cup measurements. Angularly resolved measurements are realized by installing the Faraday cup on a rotational stage and moving it on a circle centered at the ablation spot.

Supplementary to simulations with VLL, a proprietary DSMC-PIC code from the University of Stuttgart, PicLas, has been validated using results from IMD as initial parameters for plume propagation [14]. The code comprises a Direct Simulation Monte Carlo (DSMC) module for the propagation of the neutral particles of the plume whereas the self-consistent motion of the plasma is represented by a Particle-in-cell (PIC) method.

4. Target surface

The target surface before and after ablation is analyzed with a white light interferometer (Veeco NT9100). The profilometer is also used to measure the location, diameter and depth of ablation craters. Volume and mass of laser induced ablation craters can also be estimated from profilometry data [15, 9].

3. RESULTS AND DISCUSSION

A. Laser-induced momentum coupling in the µN-range

The thrust measurement data shown in Fig. 2 were measured using aluminum samples (99.9%), with a size of 25x25 mm and an rms surface roughness of 0.5 µm. All measurements used the Nd:YVO_4 laser at 1 kHz repetition rate, p-polarization and 1064 nm. The pulse energy was adjusted from 0.7 mJ to 3 mJ with a variable attenuator. The 2D galvanometer-scanner and a 420 mm effective focal length f-theta lens were used to scan the laser beam focus over an area of 21x18 mm at a line scan speed of 230 mm/s. The scan speed was adjusted to ensure that each ablation event took place on a virgin spot of target material. The laser spot size at the target was estimated as the $1/e^2$ spot size determined from a CCD camera measurement at the target position.

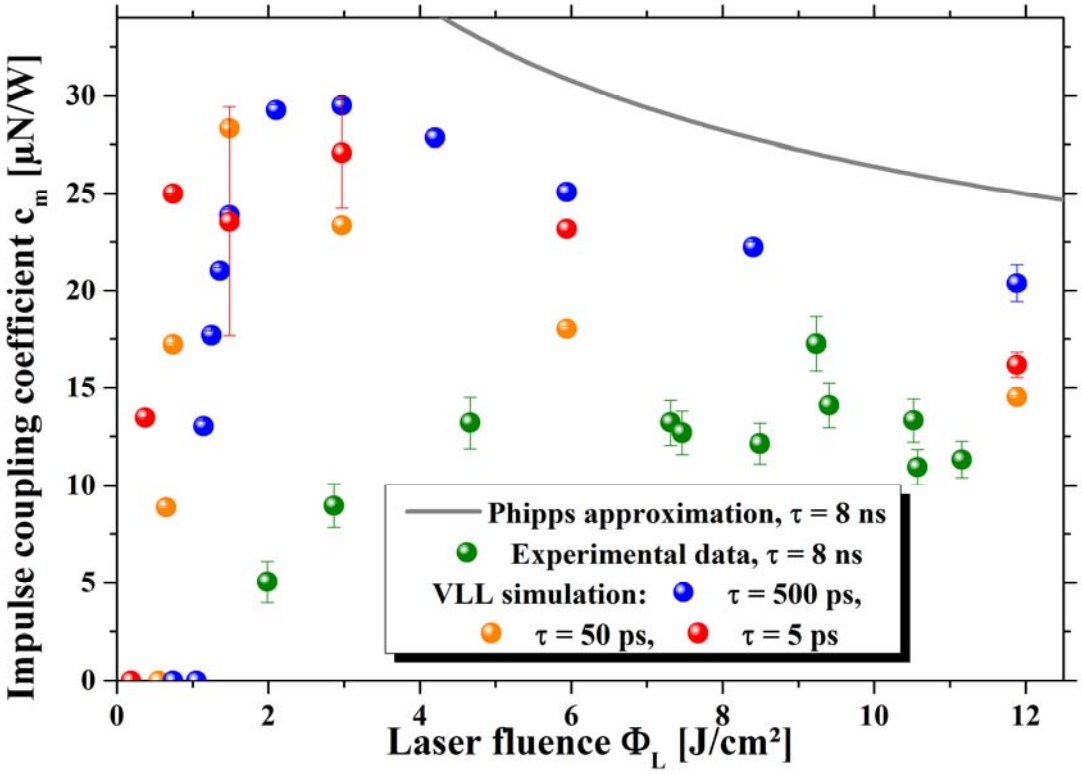

FIGURE 2. Experimental and numerical data from momentum coupling of aluminum at $\boldsymbol{\lambda = 1064\ nm}$ wavelength and $\boldsymbol{\vartheta \approx 0°}$ incidence angle. Experimental data were obtained at $\boldsymbol{\tau = 8\ ns}$, whereas simulation results depict $\boldsymbol{\tau = 5\ ps, 50\ ps, 500\ ps}$ and Phipps' trendline from [16] of c_m for aluminum alloys at pulses greater than 1 ns.

For the numerical determination of c_m, a parameter study in VLL has been carried out comprising various pulse length and fluence settings. The imparted momentum was calculated as the recoil from the approximate value of the impulse of the ablation jet, see [17] for details. Since simulations in VLL are limited from the femtosecond to the upper picosecond laser pulse range, a limited comparability of theoretical experimental results is given. Nevertheless, the shift of the optimum fluence

(maximum of c_m) and the ablation threshold towards higher fluences for longer pulses is confirmed by experimental findings. Whereas in the vapor and transition regime relatively large discrepancies between the low values of c_m and the rather high results from the simulations occur, computational findings overestimate the experimental results in the plasma regime only by a factor of 2. It should be considered here that 3D effects stemming from the spatial fluence profile in the experiment cannot be taken into account in the 1D simulation. Hence, in addition to VLL data, a trendline for laser ablation of aluminum alloys from [15] is shown for the experimental parameters. Note, that this trendline is only valid in the plasma regime which in this case is located at laser fluences above approximately 4 J/cm^2. For lower fluences and the transition to the plasma regime, however, an extended simulation is found in [18] (not depicted). Nevertheless, a fair accordance between experimental and simulation results is found.

These experimental data are relevant for impulse coupling at rather high pulse energies and serve as a proof-of-principle for thruster operation and thrust measurement. However, with respect to the target surface topology, the usage of shorter pulses will be expedient as a topic of future research. Nevertheless, as it can be seen from Fig. 2, apart from a lowered ablation threshold, the thrust characteristics are not expected to change dramatically when down-scaling the laser pulse length. In this case, molecular dynamics (MD) might be an appropriate simulation tool here [13]. Table 1 shows a first estimation on the prospective parameters of a future MICROLAS thruster using the current lasers in our laboratory.

TABLE 1. Figures of merit for a perspective MICROLAS thruster with the laboratory laser configuration: (a) 80 mW laser (TEEM Photonics) and (b) 35 W laser (Edgewave). The table shows the laser parameters pulse length τ and maximum average power P_{max} and specifications of a sample working point with its fixed parameters laser pulse energy E_L and spot diameter. The thruster characteristics are assessed by simulation results and experimental data for impulse bit and perspective thrust range.

Laser	τ	$\bar{P}_{max}$	$\mathbf{E_L}$	$\mathbf{\emptyset_{spot}}$	$\mathbf{f_{rep}}$	$\mathbf{\Delta p_{mod}}$	$\mathbf{\Delta p_{exp}}$	$\mathbf{F_{mod}}$	$\mathbf{F_{exp}}$
	$[ns]$	$[W]$	$[mJ]$	$[\mu m]$	$[Hz]$	$[nNs]$	$[nNs]$	$[\mu N]$	$[\mu N]$
(a)	0.5	0.08	0.072	30	10 … 1E3	1.536[a]	n.d.	0.015 … 1.536[a]	n.d.
(b)	8	35	3	180	10 … 5E4	84.4[b]	34	0.844 … 4221[b]	0.34 … 1700

[a] VLL simulation at $\vartheta = 15°$, p-polarization
[b] Phipps' approximation according to [15]

B. Plume diagnostics

The influence of laser angle of incidence on the plasma plume is of interest for layer-by-layer ablation of the propellant since different angles of incidence could result both from beam-steering and the changing target surface and geometry. For angularly resolved measurements of charged plume components a Faraday cup was fixed on a rotational stage and signals were measured at different angles α for the same laser and target parameters. A more detailed discussion of Faraday cup signals and the experimental setup is given in [19]. First measurements showed that single shot Faraday cup signals for the same target and laser parameters from ablation on a virgin spot on the sample are generally in good agreement both for measurements where the Faraday cup is positioned perpendicular to the sample (0°) [15] and at different

positions of 0° < α < 90° [9]. The results shown in Fig. 3 were obtained with Al (99.999%, average surface roughness ≤ 30 nm), -10 V Faraday cup bias voltage and the following laser parameters: 500 ps, 1064 nm, p-polarization, 71.7 µJ. Fig. 3 shows the integral of the filtered and averaged (5 shots) Faraday cup signals for Fig 3 a): f= 100 mm, ϑ= 15° and Fig. 3b): f= 50 mm, ϑ= 30. The distance between Faraday cup and the target was 93 mm. In the current setup the range of possible angles of incidence was limited to max. 30° and the Faraday cup could only be positioned between -5°< α < 90°. The orientation of the total plume ion component is close to α = 0°. The slight deviation from 90° in Fig. 3 a) might be due to alignment issues. Layer-by-layer ablation for long term thruster operation will require extended investigations on the influence of changing surface roughness and geometry. Measurements in a bigger vacuum chamber that will allow for a variation of the Faraday cup positions over the full 180° and also a greater range of incidence angles should give more conclusive information on this issue both for single shot and extended multi-shot experiments with different ablation patterns and laser parameters.

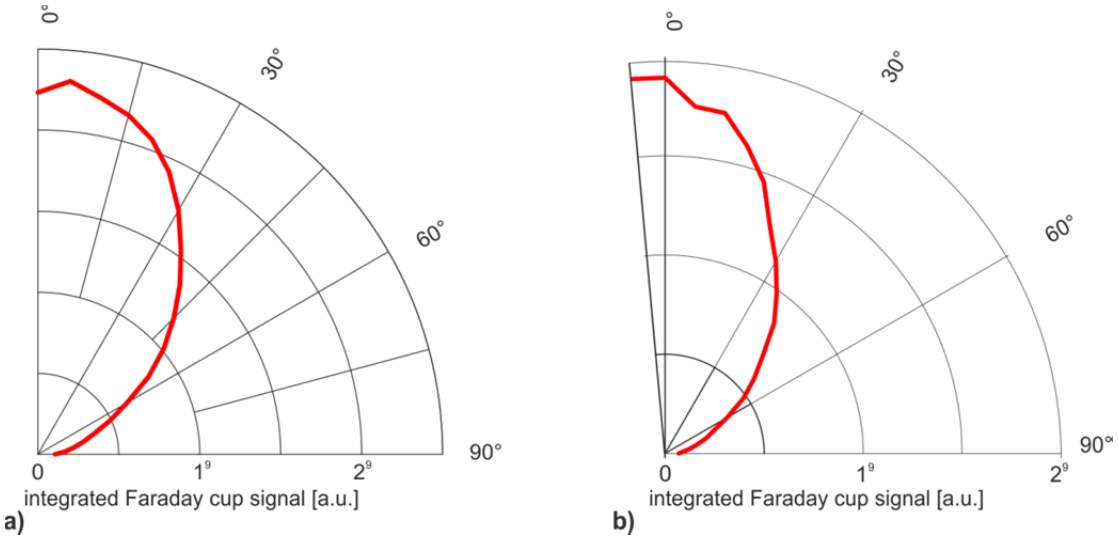

FIGURE 3. Angular distribution of the plume given by the integral of total positive charge collected with the Faraday cup for ablation of an Al target at 15° (a) and 30° (b) angle of incidence.

The Faraday cup signal from the experiments under an emission angle α = 0°, i.e., perpendicular to the target surface is shown in Fig. 4. Both jet velocity and signal strength which is equivalent to the overall mass of ionized ablated particles increase with the incident laser fluence. For a comparison with simulation results, however, the experimental data on the angular distribution of the plume have to be considered. For this purpose, the specific impulse is investigated. Using the weighted average of the particle velocities, under a certain emission angle α the velocity component perpendicular to the target surfaces yields

$$\boldsymbol{I_{sp}(\alpha) = \frac{\cos\alpha}{g \cdot Q_\alpha} \sum_t I_\alpha(t) \cdot v_\alpha(t) \cdot \Delta t} \qquad (1)$$

with

$$\boldsymbol{Q_\alpha = \sum_t I_\alpha(t) \cdot \Delta t} \tag{2}$$

which can be calculated from recorded angle distribution of the ablation plume.

Interpolation of experimental findings allows for computation of the overall specific impulse then using

$$\boldsymbol{I_{sp} = \frac{1}{g} \int_0^{2\pi} \int_0^{\pi/2} \int_0^{t_{meas}} \frac{\cos\alpha}{Q_\alpha} I_\alpha(t) \cdot v_\alpha(t) \cdot dt \cdot \sin\alpha \cdot d\alpha \cdot d\varphi} \tag{3}$$

assuming axial symmetry of the plume and orientation perpendicular to the target surface which is supported e.g. by the findings in [20].

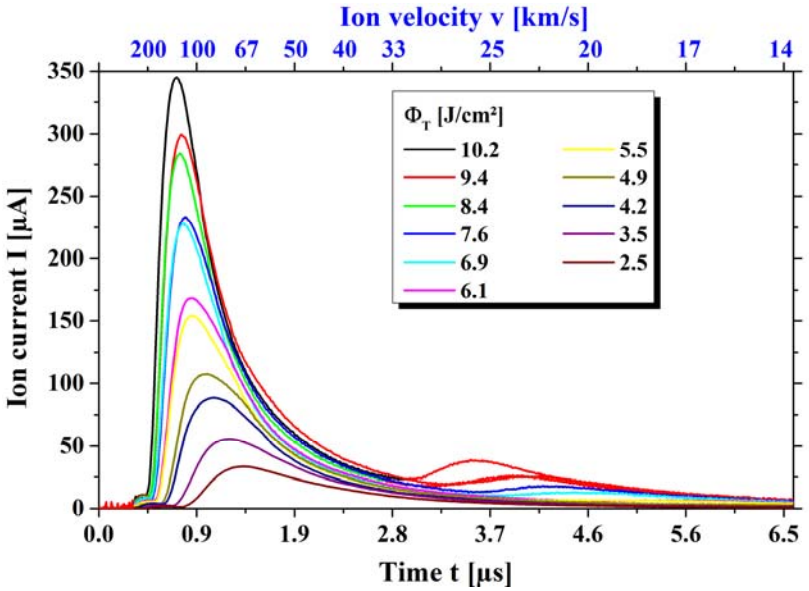

FIGURE 4. Faraday cup signal from ablation of aluminum for various fluences at the target surface with $\boldsymbol{\vartheta = 15°}$ incidence angle, $\boldsymbol{\tau = 500\ ps, \lambda = 1064\ nm}$, under an emission angle of $\boldsymbol{\alpha = 0°}$ to the surface normal, recorded at a distance of 93 mm from the ablation spot, cf. [19].

The corresponding experimental results are shown in Fig. 5. The experimental findings are underestimated by simulation results by a factor of approximately 3. It has to be pointed out that all particles including neutrals have been taken into account in the simulation whereas only charged particles can be detected by Faraday cups. However, the significant differences with respect to the distance from target in simulation (max. ~500 µm) and experiment (93 mm) leave questions on recombination on the further propagation of the plume. In general, a methodological difference is given by the temporal integration of the signal in a Faraday cup, whereas in the simulation the temporal course of the spatially integrated plume at a certain point in time is used to determine the approximate value of I_{sp}.

As an online tool, hydrodynamic simulations with VLL cover only a simulation time of around 10 ns yielding an extension of the ablation jet of approximately

500 µm, depending on the incident fluence. With respect to potential contamination of the thruster optics, however, quite larger spatial scales of around 10 cm and more are required. Moreover, determination of the plume divergence angle demands for 2D simulations at least.

Nevertheless, VLL results can serve as initial parameters of spatially resolved simulations of the plume propagation. A Gaussian laser intensity profile on the target surface was approximated by a piecewise combination of various top-hat fluences yielding data on density, velocity and temperature from VLL in the various zones of Gaussian spot. Results from DSMC simulations [10], cf. Fig. 6, are qualitatively in good accordance with model results and experimental findings from the literature.

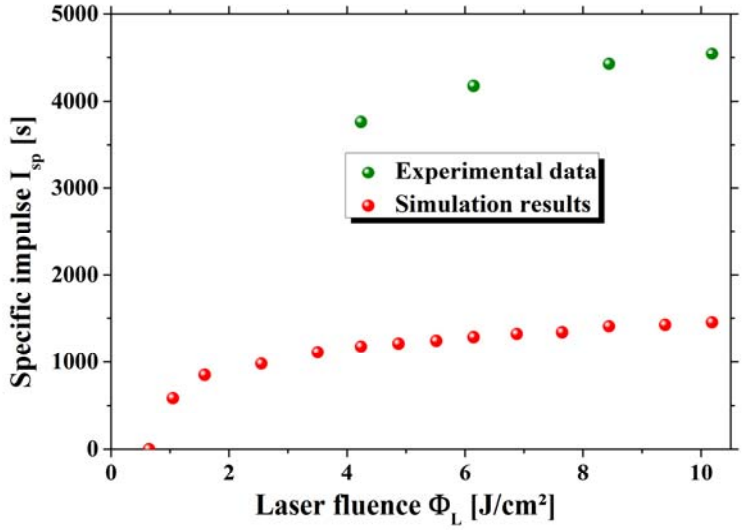

FIGURE 5. Comparison of I_{sp} derived from experimental data of the angular distribution of the ablation plume and results of hydrodynamic simulation under VLL.

As a major drawback, however, the temporal evolution describing the ablated particles moving into the simulation box is not implemented yet, but only a snapshot of the whole plume at a certain point in time deserves as initial dataset. This is as well assumed to be the main reason for the failure of the PIC part of PicLas in the present state of code development which originally was dedicated for stationary plasma flows. Hence, interaction of charged particles as well as ionization and recombination are not considered in our PicLas simulations yet.

As an alternative approach, molecular dynamics simulations might be considered as well. Though operating in a significantly smaller timescale and spatial scale, remarkably good agreements with experimental results on ablation plume characterization were reported in [21].

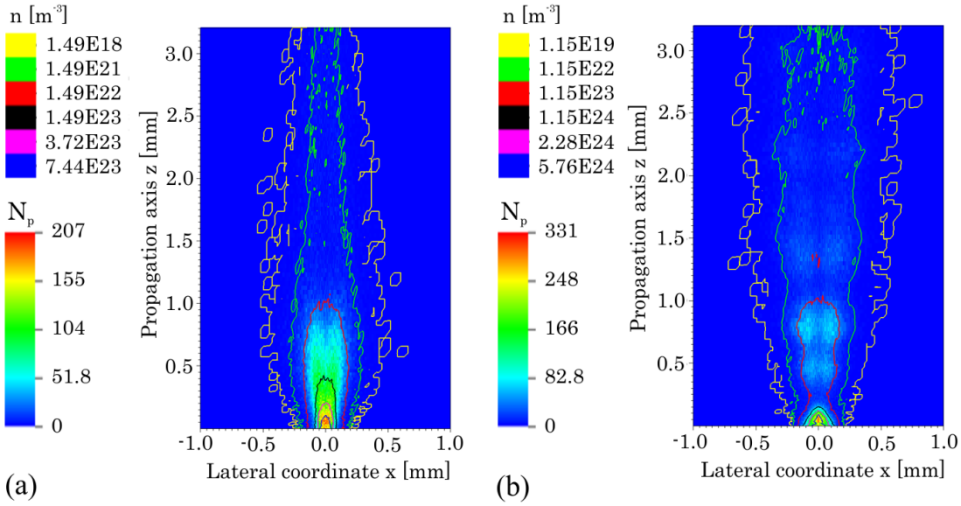

FIGURE 6. Results from DSMC simulations with PicLas (from [14]): Particle number density $\boldsymbol{n}$ (contour lines) and number of simulation particles $\boldsymbol{N_p}$ (macro particles, color gradient) at $\boldsymbol{t = 50\ ns}$ after the laser pulse peak with (a) a top hat intensity profile and (b) a piecewise combined Gaussian intensity profile of the laser spot. Initial data on $\boldsymbol{\varrho, T, u}$ were taken from VLL with $\boldsymbol{\Phi_L = 3\ J/cm^2}$, $\boldsymbol{\lambda = 1064\ nm}$, $\boldsymbol{\tau_{FWHM} = 500\ ps}$, $\boldsymbol{\vartheta = 15°}$.

C. Target surface under single and multiple shots

As reported earlier [15, 9] craters from single shot ablation events show good reproducibility for single shots on a virgin ablation spot. Additionally profilometric analysis allows for the determination of the ablation volume and hence, the ablated mass [15]. In future work, the fraction of neutrals could be calculated from experimental results, taking into account a quantitative analysis of the angular distribution of the ablation from the Faraday cup experiments. Thrust measurements would then allow for the calculation of the momentum imparted by the neutral particle fraction and therefore their mean exhaust velocity which is not detectable by Faraday cup experiments.

1D simulations only allow for a coarse estimation of the ablation depth d_a. Its anticipated upper value can be deduced by the phase-transition zone from the solid to the liquid phase. However, only a fraction of the liquid material is expelled by the ablation jet, whereas another part solidifies after the laser pulse and, moreover, a certain quantity experiences lateral expulsion to form a wall on the rim of the ablation crater, cf. Fig. 7. Hence, the 1D estimated values of $d_{a,max}$ exceed the experimental data from 3D profilometry of the maximum crater depth and the FWHM crater depth, resp. by a factor of around 2 to 6. In general, the restricted simulation time in VLL does only permit the simulation of the whole ablation process for ultrashort pulses in the range of 5 ps. The visualization of the final separation of the jet from the target, however, has not been achieved for laser pulses as long as 50 ps or more. Hence, calculations on crater depth, impulse coupling coefficient and specific impulse rely on asymptotical approximations of the temporal course.

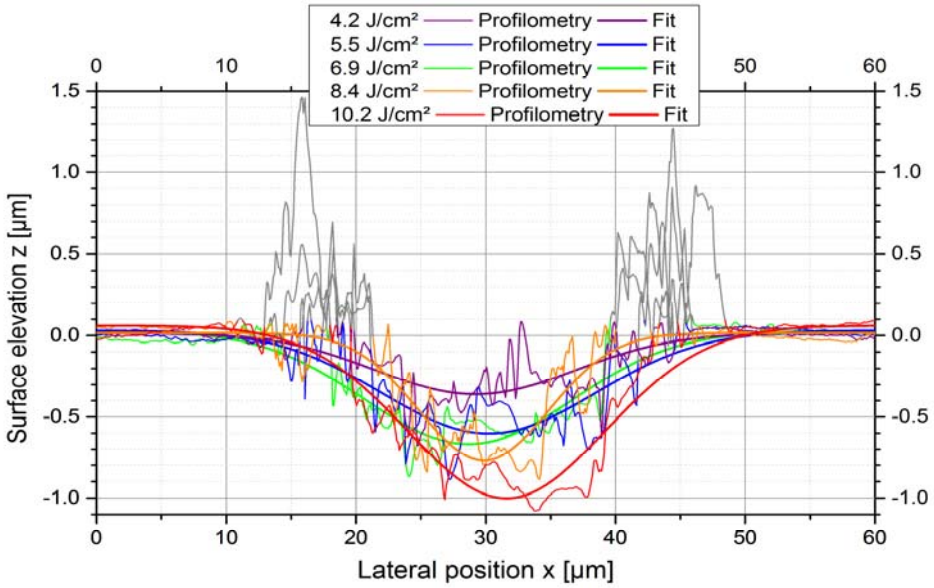

FIGURE 7. Results from profilometric analysis: Lateral x-profile of ablation craters on aluminum steeming from irradiation under various fluences and corresponding Gaussian fits of the profile neglecting the crater rim ($\boldsymbol{z > 0}$).

In fact, the successful simulation of the ablation crater shape would allow for virtual experiments of multiple shots with overlap in order to determine an adequate hatching pattern yielding reproducible flat targets even after the ablation of several layers of propellant. Given the similarity of plume characteristics as found from IMD in the nano-scale range with experimental results, as mentioned above, in principle this approach might be transferred to the topology of the target surface as well. However, for re-using a target after ablation, advanced considerations have to be taken into account here with respect to altered target reflectivity including extensive ray-tracing.

4. CONCLUSIONS AND OUTLOOK

Our research activities related to the development of a laser-ablative microthruster at DLR exhibit a great variety of experimental work and simulation models. These activities address the functionality of the thruster's components, specification of its prospective working point and especially inertia-free operation with small, reproducible impulse bits that allow for precise adjustment of thrust in the µN range with minimal thrust noise. Experimental data and computational results illustrate the complexity of this challenging task and pose the following needs for future research.

For the development of an inertia-free laser-ablative microthruster, obtaining a flat surface for each layer is essential for precise long-term operation. As known from results on laser materials processing, the appropriate selection of laser pulse length with respect to the target material is important here. Whereas nanosecond laser pulses rather result in explosive crater formation [22], laser pulses have to be shorter than the material-specific electron-phonon coupling time in order to leave a smooth surface

after multiple pulse ablation in hatching mode [5]. Therefore, the usage of shorter laser pulses, e.g. 50 ps for gold targets, 10 ps for copper, or 1 ps for aluminum, is intended to be the scope of future work.

In order to support experimental strategies, 3D simulations of laser ablation are required here. Basically, hydrodynamic simulations can be extended here, as shown in [23,24]. On the other hand, the usage of Discrete-Element-methods, as a spatial up-scaling of Molecular Dynamics, however, could provide for laser ablation simulations in the μm-range [25] within reasonable computational time.

Lateral thrust components stemming from ablation crater overlap might be a considerable source of noise with respect to the thrust direction, apart from (axial) thrust fluctuations due to the hatching mode. Hence, thorough experimental analyses on lateral components at extremely low thrust levels are required as well as sound 3D simulation. In general, however, this problem might as well be addressed by splitting the laser beam into two parts that perform separate hatching patterns on the target which exhibit point-symmetry to the target center at any time thus compensating lateral impulse components [1].

With respect to beam-steering, the realization of 2D- and 3D-scanning mode is a main topic of further developments. Beyond the proof-of-principle for inertia-free thruster operation, the incidence angle of the laser beam on the target surface has to be optimized with respect to avoidance of optics contamination by the ablation plume. Moreover, in the course of the hatching pattern under oblique incidence, refocussing of the beam at the inclined target surface and potential adjustments of the laser pulse energy due to the variation of the incidence angle should be considered.

5. ACKNOWLEDGMENTS

The authors wish to thank V. Fedotov, T. Sehnert, D. Förster, N. Dahms, and J. Mende for their scientific contribution and inspiring discussions. Moreover, thesis supervision and scientific cooperation in [13], [19] and [14] by S. Fasoulas, M. Pfeiffer, A. Mirza (Institute of Space Systems), C.-D. Munz (Institute of Aerodynamics and Gasdynamics), J. Roth (Institute of Functional Materials and Quantum Technologies), R. Weber, and A. Feuer (Institute of Strahlwerkzeuge) at the University of Stuttgart is greatly acknowledged.

REFERENCES

1. H.-A. Eckel and S. Scharring, "Tailoring Laser Propulsion for Future Applications in Space", *AIP Conf. Proc.* **1278**: 677–688 (2010).
2. C.R. Phipps, "Performance Test Results for the Laser-Powered Microthruster", *AIP Conf. Proc.* **830**: 224–234 (2006).
3. C.R. Phipps, J.R. Luke, W. Helgeson, and R. Johnson, "A ns-Pulse Laser Microthruster", *AIP Conf. Proc.* **830**: 235–246 (2006).
4. H. Dittus and T. van Zoest, "Applications of microthrusters for satellite missions and formation flights scenarios", *AIP Conf. Proc.* **1402**: 367–373 (2011).
5. J. Cheng, W. Perrie, S.P. Edwardson E. Fearon, G. Dearden, K.G. Watkins, "Effects of laser operating parameters on metals micromachining with ultrafast lasers", *Applied Surface Science* **256**: 1514–1520 (2009).
6. K. Nakamura, J. Miyazu, M. Sasaura, K. Fujiura, "Wide-angle, low-voltage electro-optic beam deflection based on space-charge-controlled mode of electrical conduction in $KTa_{1-x}Nb_xO_3$", *Appl. Phys. Lett.* **89**, 131115 (2006).
7. S. Yagi, "KTN Crystals Open Up New Possibilities and Applications", *NTT Technical Review* **7**(12), Dec. 2009.

8. T. Imai, S. Yagi, S. Toyoda, M. Sasaura, "Fast Varifocal Lenses Based on $KTa_{1-x}Nb_xO_3$ (KTN) Single Crystals", *NTT Technical Review* **7**(12), Dec. 2009.
9. S. Karg, V. Fedotov, "Investigation of laser-ablative micropropulsion as an alternative thruster concept for precise satellite attitude and orbit control", 13th ONERA-DLR Aerospace Symposium, 27th -29th May, 2013, Palaiseau.
10. S. Karg, V. Fedotov, T. Sehnert, H.-A. Eckel, "Laser propulsion research facilities at DLR Stuttgart", Presentation at the International Symposium on High Power Laser Ablation and Beamed Energy Propulsion, Santa Fe, NM, 2014 (submitted)
11. Online Simulations accessible at http://vll.ihed.ras.ru/
12. M.E. Povarnitsyn, N.E. Andreev, P.R. Levashov, K.V. Khishchenko, and O.N. Rosmej, "Dynamics of this metal foils irradiated by moderate-contrast high-intensity laser beams", Physics of Plasmas, vol. 19, 023110 (2012), http://dx.doi.org/10.1063/1.3683687
13. D.J. Förster, "Validation of the software package IMD for molecular dynamics simulations of laser induced ablation for micro propulsion", Thesis, University of Stuttgart (2013).
14. J. Peter, "Validation of the PicLas code as a numerical method for the characterization of the thruster plume in laser ablative micro propulsion", Diploma thesis, University of Stuttgart (2014) (in German).
15. H.-A. Eckel, S. Karg, and S. Scharring, "Laser Ablation Investigations for Future Microthrusters", AIP Conf. Proc. **1464**: 640 – 648 (2012).
16. C.R. Phipps et al., "Impulse coupling to targets in vacuum by KrF, HF and CO_2 single-pulse lasers", *Journal of Applied Physics* **64(3)**: 1083–1096 (1988).
17. S. Scharring, D.J. Förster, H.-A. Eckel, J. Roth, and M. Povarnitsyn, "Open Access Tools for the Simulation of Ultrashort-Pulse Laser Ablation", Poster Presentation at the International Symposium on High Power Laser Ablation and Beamed Energy Propulsion, Santa Fe, NM, 2014 (submitted).
18. C. Phipps, "An Alternate Treatment of the Vapor-Plasma Transition", *International Journal of Aerospace Innovations* **3**(1): 45–50 (2011).
19. C. Illg, "Plasma characterization for laser-ablative microthrusters for satellites", Diploma thesis, University of Stuttgart (2013) (in German).
20. A.V. Pakhomov, J. Lin, M.S. Thompson, "Ablative Laser Propulsion: An Update, Part II", *AIP Conf. Proc.* **702**: 178–189 (2004).
21. S. Sonntag, "Computer Simulations of Laser Ablation from Simple Metals to Complex Metallic Alloys", PhD thesis, University of Stuttgart (2010).
22. D. Batani, "Laser ablation and laser induced plasmas for nanomaching and material analysis", in: "Functionalized Nanoscale Materials, Devices and Systems", *NATO Science for Peace and Security Series B: Physics and Biophysics*: 145-168 (2008).
23. T. Moeller, Y.K. Chang, "MACH2 simulations of a micro laser ablation plasma thruster", *Aerospace Science and Technology* **11**: 481–489 (2007).
24. S. Kato et al., "Numerical simulation of shockwave by KrF laser ablation", *Proc. of SPIE* **4424**: 260 (2001).
25. C. Jian et al., "Experimental and Numerical Investigation of Propellant of Different Thickness for Laser Micro Propulsion", *AIP Conf. Proc.* **1230**: 186–192 (2010).